Journal of Membrane Science 378 (2011) 351–358

Contents lists available at ScienceDirect

Journal of Membrane Science

journal homepage: www.elsevier.com/locate/memsci

Geometrical influence on mixing in helical porous membrane microcontactors

Jigar M. Jani [a], Matthias Wessling [b], Rob G.H. Lammertink [a,*]

[a] Soft Matter, Fluidics and Interfaces, MESA+ Institute for Nanotechnology, P.O. Box 217, 7500 AE Enschede, The Netherlands
[b] Membrane Science and Technology, P.O. Box 217, 7500 AE Enschede, The Netherlands

ARTICLE INFO

Article history:
Received 22 March 2011
Received in revised form 10 May 2011
Accepted 12 May 2011
Available online 20 May 2011

Keywords:
Gas–liquid contactors
Optimization
Membrane microreactor
Micromixers
Porous membrane

ABSTRACT

The goal of gas–liquid micromixing has led to develop various kinds of passive micromixer configurations, which can be used for many microfluidics applications. This work details gas–liquid contacting using porous helical microchannels. An experimental and numerical design methodology for different geometrical configurations is presented which systematically integrates computational fluid dynamics (CFD) with an optimization methodology based on the use of design of experiments (DOE) method. The methodology investigates the effect of geometric parameters on the mixing performance of helical membrane microchannel that has design characteristics based on the generation of secondary vortices. The methodology has been applied on different designs of helical hollow fiber geometry at several Reynolds numbers. The geometric features of this microchannel geometry have been optimized and their effects on mixing are evaluated. The flux enhancement and degree of mixing are the performance criteria to define the efficiency of the gas–liquid microchannel contactor for different design requirements. Due to its ease of fabrication, efficiency and operational flexibility, helical membrane micromixers are favorable for gas–liquid contacting, water oxygenation, pervaporation, etc.

1. Introduction

Process intensification by innovative process design is the preliminary way to achieve less emission, improved chemistry and enhanced process efficiency. Microchemical technology has been widely studied for precise chemical synthesis while achieving downsized chemical plants. This miniaturized chemical plant consists of micromixers, heat exchangers and microreactors.

An important field of application for micromixers is gas–liquid reaction technology, which has attracted great amount of attention in recent years. For gas–liquid reaction, often multiphase catalysis is employed to reduce the reaction temperature and minimize unwanted side products. This type of gas–liquid–solid reaction could be carried out in various types of reactors i.e., dispersed phase reactors, falling film microreactors, micro-packed bed reactors and microreactors with interfaces stabilized by physical structures (membranes, micro-porous plates, etc.) [1].

In microfluidic systems, analytical and experimental studies show that capillary forces dominate over the body forces (viscous and pressure forces) existing in the system [2]. In droplet based microfluidics, droplets of the fluids are generated and as they move along the microchannel, an internal flow field is generated. This causes enhanced mixing near gas–liquid interfaces [3–9]. There are numerous studies of physical aspects of droplet microfluidics in microchannels tuning the wetting condition at the wall and the way droplets move in microchannels [10]. Membrane based gas–liquid contacting can be useful to achieve a stable gas–liquid interface [11]. These membrane microreactors contain hydrophobic membrane structures with small pores typically around 50–100 nm. They act as a porous support to facilitate contact between gas and liquid phase. Here, the porous membrane must be non-wettable to ensure that the liquid does not fill the pores. With this approach, gas and liquid will remain in contact with each other at the microchannel wall.

For gas–liquid catalytic reactions using porous membranes, a stable interface can be formed. In such microreactor devices, the gas and liquid reactants have to diffuse to the catalyst surface [12]. For relatively slow reactions, concentration gradients due to transport limitation will be small. For fast reactions, the overall reaction rate will become limited by the transport of reactant from bulk liquid phase to the catalyst surface. In order to achieve high mass transfer rates, mixing in the liquid near the liquid–solid interface is necessary.

Micromixers are classified in two categories: active and passive micromixers. Actuated components in active micromixers require external power to achieve mixing. A passive micromixer makes use of geometrical configuration in order to increase the interfacial area between the fluids which in turn increases the mixing performance. One of the big advantages of passive micromixers is its ease of fabrication and its operational simplicity compared to

* Corresponding author. Tel.: +31 53 489 4798; fax: +31 53 489 2882.
E-mail address: r.g.h.lammertink@utwente.nl (R.G.H. Lammertink).

0376-7388/$ – see front matter © 2011 Elsevier B.V. All rights reserved.
doi:10.1016/j.memsci.2011.05.021

active micromixer. Different methodologies were adapted for passive micromixers to achieve higher mixing efficiencies [13–15]. A comprehensive knowledge of the underlying physics is very essential for the optimal design of these microdevices.

Typical dimensions of these microdevices are in sub-millimeter range and thus, conventional methods to create mixing are not feasible. The Reynolds number for flow of fluids in these devices is defined as;

$$Re = \frac{du}{\nu} \tag{1}$$

where, u is the average flow velocity, d is the characteristic channel dimension and ν is the kinematic viscosity of fluid. Due to very small characteristic dimension of the microchannel and low velocity, Re is very small. This implies that mixing is mainly observed due to molecular diffusion and not mainly by convection.

Further, the Peclet number is defined as;

$$Pe = \frac{du}{D_{\mathrm{mol}}} \tag{2}$$

where D_{mol} is molecular diffusivity. A typical Pe value in microchannels is 1000 or larger, which indicates that diffusive mixing occurs at much lower rate than the typical timescales involved for convective fluid flow. The mixing length is proportional to Pe for laminar unidirectional flow. Corresponding mixing length can be in the order of several centimeters. This leads to longer microchannels for complete mixing [16]. In several membrane applications, enhanced mixing performance using Dean vortices and generation of secondary flows have already been demonstrated [17]. In helical microchannels, transverse secondary flows arise as a result of the counter acting forces of centrifugal and viscous forces. Centrifugal force depends quadratically on the average velocity, u, while the viscous force depends linearly on u. Therefore, secondary flows get severely dampened at lower velocities. However, at larger fluid velocities (at $Re \geq 10$), centrifugal forces become stronger, promoting the secondary flows. This effect brings advantage to gas–liquid contacting using porous membranes as the gas reactant enters from the porous wall. Secondary flows can be induced in curved channels provided that complex 3D geometries are employed [18,19]. They have determined the parameters that control fluid stirring in the channels with no moving parts. The results of numerical studies indicate the stretching of material lines and three-dimensional trajectories of fluid particles. Their study indicates coupling between chaos in the transverse direction and the non-uniform longitudinal transport of materials. Fig. 1 shows the geometric parameters of the helical micromixer. The Dean number Dn is commonly regarded as a dimensionless number for flow description in a curved channel. It describes the ratio of centrifugal forces to viscous forces. It also takes into account the geometrical characteristics of the microchannel:

$$Dn = Re\sqrt{\frac{d_i}{d_c}} \tag{3}$$

where, d_i is the characteristic channel internal diameter and d_c is the curvature diameter of the curved microchannel. To include the helical pitch effect on the Dean number, the modified helical coiled diameter is taken into account [20]. It is defined as:

$$d_c{}' = d_c\left(1 + \left(\frac{p}{\pi d_c}\right)^2\right) \tag{4}$$

Based on Eq. (4), the modified Dean number is calculated as;

$$Dn' = Re\sqrt{\frac{d_i}{d_c{}'}} \tag{5}$$

At the beginning of the channel the flow conditions are parabolic and laminar, until it becomes influenced by centrifugal forces inducing secondary vortices. An important parameter which defines the developing length θ (°) [21] describing fully developed secondary flow can be written as;

$$\theta = 87.3\left(Dn\frac{d_i}{d_c}\right)^{1/3} \tag{6}$$

In many membrane separation processes, these secondary flows are used in order to enhance mass transfer. The study of helical flows and mixing due to chaos in curved geometries has been performed experimentally and numerically [22–24]. The experimental results verify that the mixing effect is deeply related to the structure of helical flow patterns formed inside the micromixer [25]. They also quantified the mixing with different flow parameters. Several numerical and experimental studies have been performed to study the efficiency of helically wound hollow fiber modules [26–29]. They have compared the limiting flux, energy consumption and the effect on mass transfer by shear stress in helical hollow fibers. The relationship between variations in local velocity components and wall shear stress has been established. That allowed authors to observe the evolution of Dean vortices induced by flow and geometry variations.

To date, there have been a number of theoretical, experimental and numerical studies aimed at the optimization of twisted and grooved micromixers [19,30–32]. However, systematic design and optimization approach for gas–liquid contacting in porous helical membrane contactor was not performed till date and this research aims to address this problem. This work also aims to present quantification of total gas uptake in liquid numerically and experimentally for different module configuration. In this study, gas uptake experiments and numerical analysis were performed for liquid flowing inside various microchannels at different flow velocities. A detailed experimental and numerical approach for design and optimization of micromixers is presented that inte-

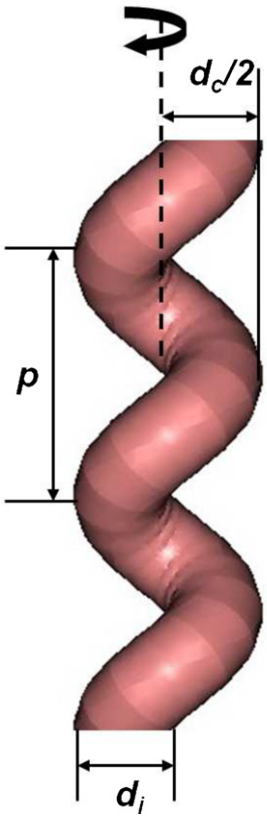

Fig. 1. Schematic of geometrical parameters of helical microchannel.

grates computational fluid dynamics (CFD) with Taguchi method [33] of optimization (based on design of experiment). A full experimental and numerical study details the magnitude of secondary flow in helical microchannel for different operating and geometrical parameters, where optimized parameters can be used to optimize flow within this membrane micromixer.

2. Experiment

2.1. Materials

Pure oxygen and nitrogen were obtained from Praxair, Belgium. Demineralized water was used for the operation.

2.2. Module preparation and fluidic setup

The hollow fiber membranes used in micromixer modules were composed of porous, microfiltration Accurel S6/2 polypropylene (PP) – purchased from Membrana GmbH (Germany). These fibers had an outer diameter of 2.7 mm, an inner diameter of 1.8 mm and according to the supplier an average pore size of 0.27 μm. Two kinds of micromixer modules were prepared: straight and helically wound. The micromixer module was housed into a glass tubing. The circular glass shell has inlet and outlet ports for the connections. The fiber was tied at regular intervals around the glass rod and later placed into the glass shell. The fiber, at the ends of the glass tubing, was glued using polyurethane glue. The helically wound hollow fiber module was prepared manually adjusting curvature diameter and helical pitch on glass rod with regularly spaced ties on it. The geometrical specifications for the helically wound and straight hollow fiber modules were shown in Table 1.

Fig. 2 displays schematic representation of the experimental setup for hollow fiber membrane micromixer module. The setup consists of a programmable syringe pump (Harvard Apparatus, accuracy within 0.35% and reproducibility within 0.05%), an oxygen sensor (PreSens Fibox 3, accuracy ±0.15% air-saturation at 1% air-saturation, resolution 1 ± 0.05% air-saturation), mass flow controller (Bronkhorst, accuracy ±0.5% of reading plus ±0.1% full scale) and a PC for the data acquisition. PEEK tubings (3.175 mm OD, P-1534) and fittings (3.175 mm OD, P-100) from Upchurch Scientific were used for the connections.

Table 1
Generalized geometrical dimension for porous gas–liquid micromixer module used in experiments.

Geometric parameters	Dimensions
Channel length	180 mm
Channel internal diameter	1.8 mm
Helical pitch	40 mm
Helical curvature diameter	2.5 mm
Average pore size	0.27 μm
Membrane thickness	0.45 mm

2.3. Gas–liquid contacting experiments

To evaluate the performance of micromixer under different geometrical conditions, the hollow fiber membrane module was subjected to different flow conditions. The feed water was injected at flow rates ranging from 0.05 mL/min to 10 mL/min through the lumen side of the fiber. Pure oxygen was supplied to the shell of the glass tubing.

The feed water was continuously bubbled with inert nitrogen gas (in a separate vessel) in order to remove the oxygen. The oxygen content in the liquid outlet was monitored. Apart from that, the oxygen content in the degassed water was also monitored using an oxygen sensor. The driving force for the oxygen transfer varies with the axial position in the module and it drops along the length of the micromixer. An expression for the overall oxygen flux at the microchannel outlet, N, can be expressed by,

$$N = \int \frac{4Q(r)c(r)dr}{\pi d_i^2} \tag{7}$$

where $Q(r)$ and $c(r)$ are liquid flow rate and oxygen concentration, respectively. Hollow fiber radius and internal diameter of the microchannel are denoted as r and d_i, respectively. The experiments were carried out at ambient pressure and temperature conditions.

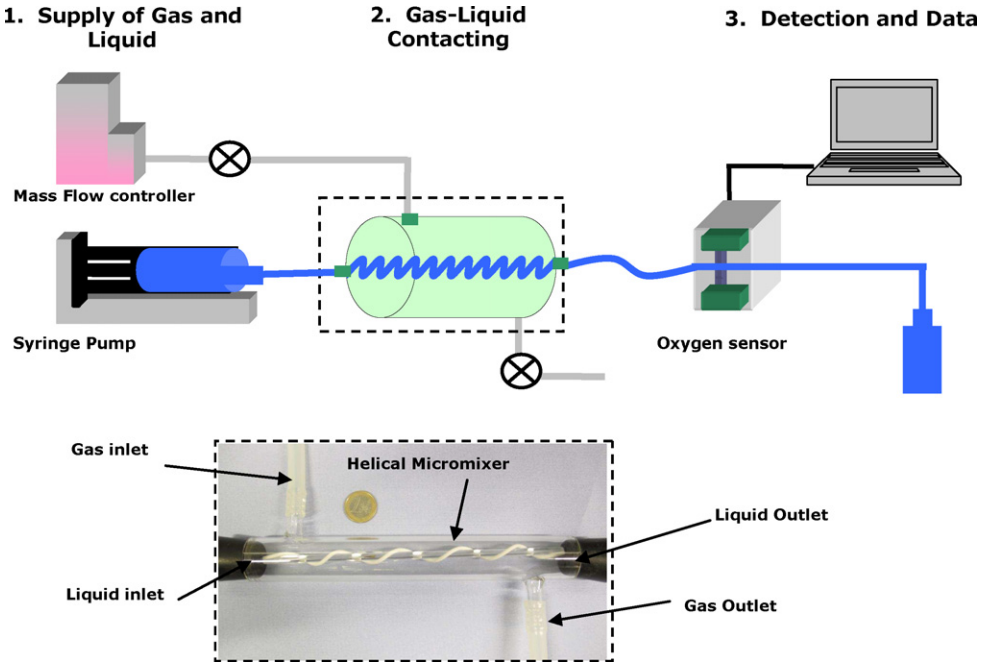

Fig. 2. Schematic representation of experimental setup used for O_2 uptake into water.

Table 2
Properties of the fluids at 20 °C.

Fluid	Density (kg/m^3)	Viscosity (kg/m s)	Diffusivity (m^2/s)
Water	9.98×10^2	0.9×10^{-3}	1.0×10^{-9}
Oxygen	1.429	0.20×10^{-6}	2.00×10^{-9}

3. Numerical analysis

For detailed understanding of fluid flow, mixing and micromixer performance, computational fluid dynamics (CFD) simulations were performed using COMSOL Multiphysics 3.5. Gas–liquid contacting in porous helical microchannels was modeled incorporating different geometrical parameters. All simulations were performed in steady state for three-dimensional mode. For optimum computational power, convergence and accuracy, the unstructured tetrahedral mesh was varied between 215,000 and 250,000 elements (Lagrange type p2, p1), depending upon the dimension of the microchannel. The mesh has been refined until the numerical observations were consistent. The mesh size was smaller near the membrane wall to capture concentration variations accurately. Tetrahedral mesh does not pose any constraints on the structure of the geometry. Hence, it can be used to mesh sharp curvatures of the helical geometry. The accuracy of the result was further increased by adjusting the geometry resolution. This numerical model solves the Navier–Stokes equation coupled with convection–diffusion equation using the finite element method. The governing equations are represented as follows:

$$\nabla \cdot u = 0 \tag{8}$$

$$\rho[(u \cdot \nabla)u] = -\nabla P + \eta \nabla^2 u \tag{9}$$

$$D\nabla^2 c = u \cdot \nabla c \tag{10}$$

Here, ρ and η are the density and viscosity of the liquid and D is the diffusion coefficient. Pressure, oxygen concentration and time are denoted as P, c and t, respectively. Physical absorption of oxygen into water is selected as the test case. Water is flowing inside the microchannel and oxygen diffuses through the porous membrane. Geometrical dimensions of the helical micromixer for CFD studies were kept same as the experimental module (shown in Table 1). The physical properties of the gas and liquid at 20 °C are mentioned in Table 2.

For the boundary conditions, a fully developed parabolic flow profile has been implemented at the microchannel inlet and the outlet is kept at normal pressure. There will be zero oxygen concentration at the microchannel inlet and convective flux will be implemented at the outlet boundary. The wall boundary conditions are defined as follows:

1. For Navier–Stokes application mode, wall velocities will be zero (no-slip condition).
2. For convection–diffusion application mode, saturated wall boundary condition will be implemented to simulate gas uptake through the hydrophobic porous wall.

The mixing cup concentration of absorbed gas into the liquid from the microchannel outlet was compared with the experimental results.

4. Optimization method

It is essential to choose appropriate design parameters and their range of variations for proper description of the design objective. Mixing index or mixing intensity is the major performance parameter for the design of any micromixer. This quantification is possible by calculating the variance of the component in the micromixer.

Table 3
Orthogonal array (OA) L_9.

Design of experiments (DOE) for CFD studies	Design parameters		
	A	B	C
1	1	3	3
2	1	1	1
3	1	2	2
4	2	3	1
5	2	1	2
6	2	2	3
7	3	3	2
8	3	1	3
9	3	2	1

The variance σ and mixing index M of the species concentration on the cross-section normal to the flow direction are defined as;

$$\sigma = \sqrt{\frac{1}{m}\sum (c - c_\infty)^2} \tag{11}$$

$$M = 1 - \frac{\int_A |c - c_\infty|\, dA}{\int_{A_0} |c_0 - c_\infty|\, dA} \tag{12}$$

where m is the number of the sample points for a given cross-section, c is the local (area element) value of the concentration of one fluid species on the selected cross-section plane A, c_0 is the local concentration at the inlet plane A_0 (which is zero) and c_∞ is the concentration of complete mixing (mixture steady-state concentration). The mixing index is 1 for complete mixing and 0 for no mixing.

One of the important factors affecting the precision of the design methodology is the choice of geometrical design variables and its variation range. The Taguchi method of optimization is based on orthogonal array (OA) experiments and gives reduced variance for well-balanced experiments with optimum settings of parameters. Principally, some preliminary tests are necessary for sensitivity analysis which gives tentative range of design variable before proceeding towards detailed design. An experimental table of 9 designs was formulated by using the OA L_9 of the Taguchi method. The orthogonal array showing L_9 formulation is shown in Table 3. To realize this formulation, three design parameters with three levels were chosen. Table 4 shows the ranges and values of the geometrical design parameters taken in our study. For all models used in the optimization study, the total length of microchannels is fixed at 60 mm.

The mixing of gas into the liquid in these 9 different designs were studied by CFD analysis at various Reynolds numbers. For evaluating the influence of the design parameters on mixing index, Taguchi method's signal-to-noise ratios (S/N) are used.

The S/N ratios are defined as log functions of the desired output which can help understanding the desired output and detailed data analysis. In order to calculate S/N ratio from the simulation results,

Table 4
Design parameters and levels used in OA L_9 (all values shown in the table are in mm).

Levels	Factors		
	Curvature diameter A	Helical pitch B	Internal diameter C
1	2.5	20	1.0
2	3.5	30	1.5
3	4.5	40	2.0

Eq. (11) is used at the outlet of the microchannel which can be later used in Eq. (13):

$$n = \frac{S}{N} = -10 \log\left(\frac{1}{\sigma^2}\right) \quad (13)$$

For the optimal output for the performance parameter, S/N ratio should be maximized. The mean of S/N ratios of the design experiments of OA L_9 were calculated to evaluate the contribution of each level to the mixing index.

5. Results and discussion

5.1. Description of the system

Straight and helical membrane modules were fabricated using Accurel S6/2 polypropylene (PP) hollow fibers. Water is flowing inside the hollow fiber microchannel and oxygen is continuously fed at the shell side. This allows oxygen transport across the membrane from the shell side to the water. The outlet oxygen concentration in the water was constantly monitored by an oxygen sensing probe.

5.2. Oxygen uptake

Oxygen uptake in porous membrane microchannels was evaluated by both oxygen absorption experiments and COMSOL simulations. To study the effect of helical microchannel geometry, a helical microchannel was compared with an equivalent length (180 mm) of a straight porous microchannel module. Fig. 3A displays outlet oxygen concentrations of straight and helical microchannels for both experiments and simulations (oxygen saturation concentration is 40 mg/L at 25 °C and 1 bar). The outlet oxygen concentration in helical hollow fiber modules is higher than the straight ones. For low *Re* (below 5), the liquid gets saturated almost completely. The experimental results obtained at lower *Re* display large variations compared to the numerical results. This difference can be explained by the experimental error incurred due to the low liquid flow rates. The overall flux enhancement in a helical microchannel compared to the straight channel is shown in Fig. 3B. The results, both from the COMSOL models and oxygen absorption experiments, show higher oxygen absorption for the helical microchannel compared to the straight channel.

As liquid flows at higher *Re* through the helical microchannel, the secondary flow perpendicular to the flow direction increases. This counter-rotating recirculation along the microchannel induces more gas absorption compared to the straight microchannel. It has been observed that with the secondary flow in helical microchannel at higher *Re* (above 60), more than 80% enhancement in overall flux can be obtained compared to the straight channel.

5.3. Mixing in helical membrane microchannel

Numerical simulations were performed to study mixing and mass transfer in helical microchannel. Fig. 4 shows the mixing index for a helical microchannel (d_c = 1.5 mm, p = 15 mm, d_i = 1.0 mm) and a straight microchannel for different values of Reynolds number (0.5–150). At lower *Re* (higher residence time), gas will diffuse till the center of the microchannel and the liquid will get saturated with gas within a few millimeters of channel length. As *Re* is increased the residence time gets shorter, which reduces dissolution of gas into the liquid for both geometries. In a straight microchannel gas uptake will be purely based on the diffusion and an increase in *Re* leads to drop in mixing. However, when *Re* is increased, the helical microchannel will induce Dean effect. It is observed from the figure that, at higher *Re* for the same values of internal diameter

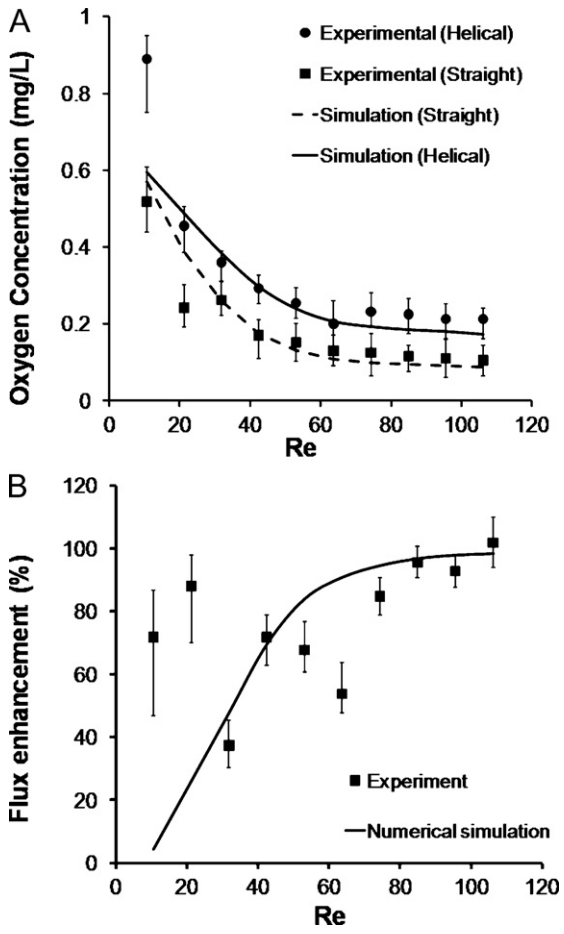

Fig. 3. Oxygen uptake. (A) Oxygen outlet concentration against *Re*. (B) Flux enhancement *vs Re*; experimental values are shown in dots and simulation values are shown in line.

and microchannel length, the mixing in a helical microchannel is enhanced compared to a straight microchannel.

It is evident from the numerical simulations that the curved geometries, because of their specific design, trigger transverse secondary Dean flows as a result of interplay between inertial and centrifugal forces. The intensity for such secondary flows increases as the fluid is pushed back from the outer wall to the inner wall of the microchannel at higher liquid velocities as previously demon-

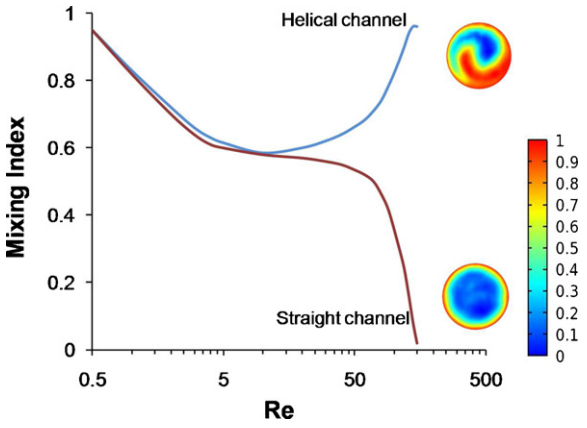

Fig. 4. Mixing using helical microchannels. Mixing index *vs Re* comparing helical microchannel (d_c = 1.5 mm, p = 15 mm, d_i = 1.0 mm) with equivalent length of straight channel. Also showing simulation results of outlet oxygen concentration distribution at *Re* = 100 for both helical and straight microchannel.

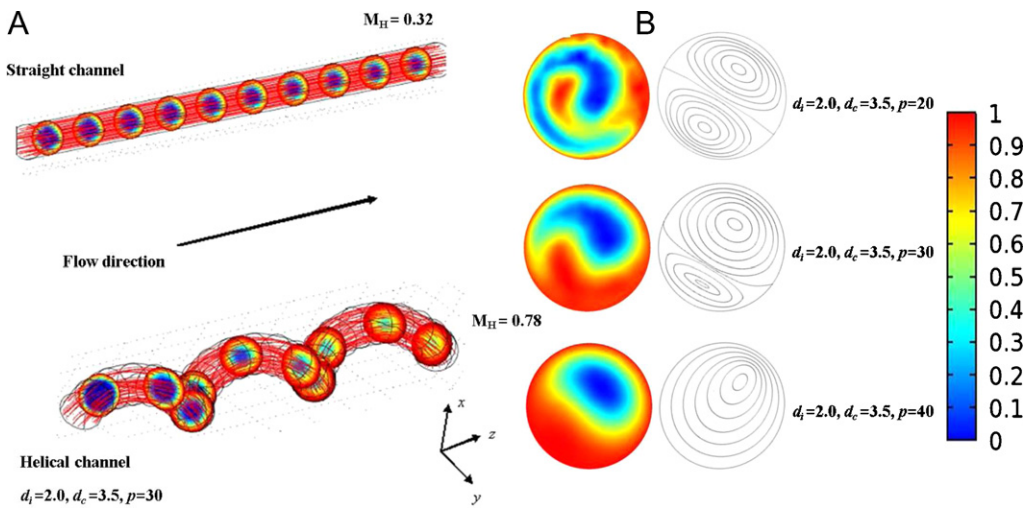

Fig. 5. Comparison of concentration distribution between helical and straight microchannel (A) axial concentration profile (B) cross-section concentration plot (on left) after first rotation (360°) and velocity contours (on right) for three different geometries.

strated by Moulin et al. [26] by means of laser visualization. At lower flow rates ($Re < 3$), secondary flows are not dominant so that it can perturb the parabolic laminar flow.

The degree of mixing increases along the axial flow direction for the helical microchannel compared to the straight channel at $Re = 50$ (Fig. 5A). The mixing index at the outlet of the microchannel clearly demonstrates enhanced mixing in the helical microchannel. Fig. 5B displays the axial and radial in plane velocity profile at constant Reynolds number ($Re = 50$) for three different geometries. The velocity changes (for fully developed secondary vortices) is observed around $\theta = 240°$ for helical channel ($d_c = 3.5$ mm, $p = 20$ mm, $d_i = 2.0$ mm). The developing length calculated based on Eq. (6), for the same flow conditions and geometry, gives $\theta = 243.11°$ as developing length, which is in good agreement with our numerical results. Two counter-rotating vortices are observed at lower helical pitch ($Re = 50$, $Dn = 37$). For higher helical pitch (40 mm), the axial velocity profile is pseudo-parabolic and there are only small rotating vortices in the secondary flow. When the helical pitch is decreased, the velocity profile also changes. At the identical Reynolds number, for smaller pitch (also for curvature diameter), the representation of axial velocity (orthogonal to the flow direction) suggests that slowly the flow gets away from the center of the channel towards the inner wall of the microchannel.

5.4. Optimization of geometrical parameters

The effects of curvature diameter, helical pitch and internal diameter were investigated numerically. The application of optimization study using an orthogonal array gave the influence of the design parameters on performance criterion-mixing index. To evaluate the contribution of each level of a design parameters on the S/N ratio of the mixing index, the mean of the S/N ratios of the experiments in the OA L_9 is calculated according to Eq. (13). According to the definition of S/N ratio, larger-the-better was the constraint in selecting the crucial parameters. The mixing index for equal residence time in different geometries at a wide range of Reynolds numbers is plotted in Fig. 6.

The optimization study gave the optimal geometry for improved gas–liquid contacting in a porous helical membrane modules. Mixing index of the optimal geometry was compared to different microchannel geometry configurations. It can be seen that the mixing index at very low Re (0.5, high residence time) is near unity due to saturation of the gas into the liquid. As the Reynolds number increases (lower residence time), the mixing index drops gradually to a minimum (different minimum for different geometries) for all geometries. This is due to lower amount of gas uptake into the liquid (owing to shorter residence time). However, after this critical Reynolds number ($Re = 3$, $Dn' = 0.42$), two counter-rotating secondary vortices start to develop because of the Dean effect. This result is in agreement with previous work of Moulin et al. [28], which showed that secondary vortices can be observed at such very low flow rates ($Re = 1$, $Dn' = 0.4$). These secondary flows enhance gas absorption near the gas–liquid interface. This effect provokes gas absorption when the Reynolds number is further increased leading to further enhancement in the gas uptake. This can be seen as an increase in the mixing index in Fig. 6.

It is evident (Fig. 6A) that the smallest helical pitch (20 mm) gave maximum mixing at any given Re. Recirculation inducing transver-

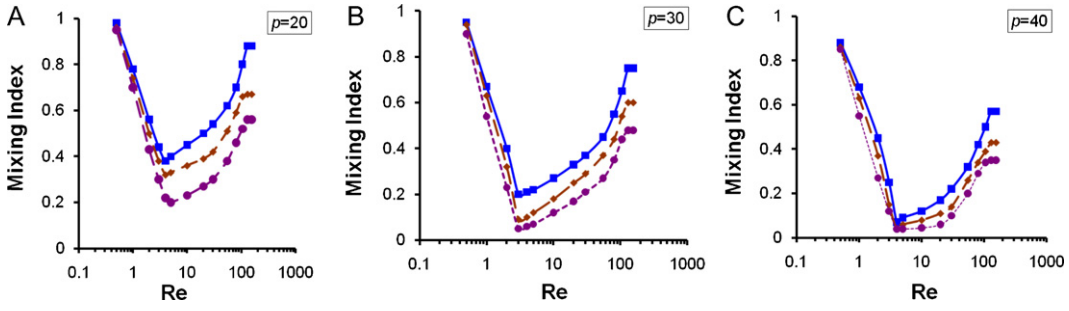

Fig. 6. Influence of helical pitch and curvature diameter on mixing at different flow rates. -■- shows results of $d_c = 2.5$ mm, $d_i = 2.0$ mm, -♦- represents $d_c = 3.5$ mm, $d_i = 2.0$ mm and -●- shows $d_c = 4.5$ mm, $d_i = 2.0$ mm for (A) $p = 20$ mm (B) $p = 30$ mm (C) $p = 40$ mm.

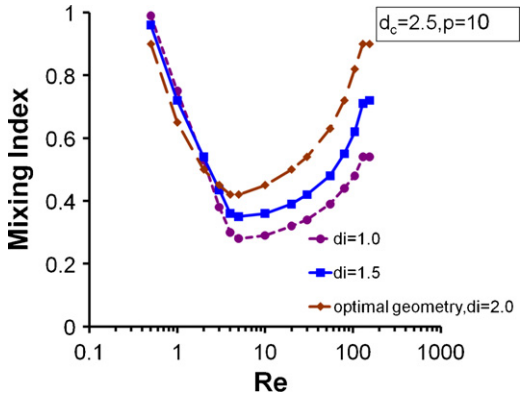

Fig. 7. Mixing index *vs Re* for helical microchannel with with different internal diameter for $d_c = 2.5$ mm, $p = 10$ mm.

sal velocity that instantaneously transports absorbed gas from the gas–liquid interface to the center of the microchannel. It is also very clear (Fig. 6A–C) that mixing increases with increased curvature. The microchannel with higher curvature pushes liquid from the outer wall towards the inner wall faster than the microchannel with smaller curvature. It is also interesting to see from the plots in Fig. 6 that for the smaller pitch (20 and 30 mm), the minimum in the mixing index for different design configurations is distinct and separate. The minimum of mixing index for the optimized geometry is higher than the other configurations. However, as the helical pitch is increased (40 mm), the distinctive nature is less pronounced. This is because of dampened Dean effect due to the larger helical pitch. This clearly shows that in order to achieve higher mixing, both helical pitch and curvature diameter should be reduced.

The influence of internal diameter on mixing is shown in Fig. 7. The micromixers with larger diameters (2.0 mm) show lower gas uptake at lower range of *Re*, this is because of a longer diffusion path. At higher *Re*, as the internal diameter of the microchannel increases, the mixing effect also increases due to centrifugal force acting on the fluid element near the microchannel wall. The reason for this can be the centrifugal force acting on the fluid near the channel wall that is higher than the fluid element near the center of the channel. And as the channel radius increases, recirculation near the channel wall increases. This leads to higher gas uptake in the liquid near the microchannel wall. This explains the increase in the mixing for increasing the micromixer internal diameter. Thus, according to Figs. 6 and 7, it can be deduced that A1B1C3 is the optimized geometry giving the highest mixing. However, this optimized design is located in the constraints set for the experimental conditions. Improved design methodology with wider range of critical design parameters is warranted in order to study the entire design space.

6. Conclusions

One of the main goal of the this work was to optimize a gas–liquid micromixer that was fairly simple, efficient and easy to operate. This way a new concept for gas–liquid contacting in porous helical membrane microchannels has been developed. It was demonstrated that helical structures perform more effectively compared to the straight microchannel. This has been analyzed using both numerical and experimental methods. The oxygen uptake experiments were performed in straight and helical microchannel to show gas–liquid contacting efficiency in both geometries. The helical design geometry has been exploited to produce secondary flows in microchannels. This significantly reduces complex micromixer fabrication methods and need for auxiliary equipments. This work clearly shows that the measured gas uptake in liquid flowing inside helical membrane microchannel was higher compared to the straight microchannel. Flux enhancement was more than 80% in helical microchannel compared to the straight channel for Reynolds number more than 60. It also suggests that the flux enhancement is not only dependent on Reynolds number but it also depends strongly on the geometrical configuration of the microchannel. The numerical study was performed on detailed optimization to study the influence of geometrical parameters on the performance of gas–liquid helical microcontactors and to maximize the mixing. The objective was to maximize the mixing index using three design variables. i.e., the curvature diameter, helical pitch and channel internal diameter. The design parameter sensitivity analysis suggested that mixing is more sensitive to the curvature diameter and helical pitch. Increase in internal diameter of the microchannel increases mixing because of pronounced Dean effect due to centrifugal force. The results from geometric optimization and numerical study showed that the degree of mixing has been significantly improved with modification of the channel curvature diameter and helical pitch. The obtained results are relevant for detailed understanding of gas–liquid contacting applicable to membrane based processes, where the knowledge of optimization of hollow fiber geometry provides useful information which can be implemented to overcome mass transport problems.

Acknowledgment

This work was financially supported by Netherlands Research Organization-STW project. The authors also greatly acknowledge H.C. Aran and D. Salamon for fruitful discussions.

References

[1] V. Hessel, P. Angeli, A. Gavriilidis, H. Löwe, Gas–liquid and gas–liquid–solid microstructured reactors: contacting principles and applications, Ind. Eng. Chem. Res. 44 (2005) 9750–9769.
[2] C. Kim, Proc. Symp. Micromachining and Microfabrication, 1999, p. 4177.
[3] T. Thorsen, R. Roberts, F. Arnold, S. Quake, Dynamic pattern formation in a vesicle-generating microfluidic device, Phys. Rev. Lett 86 (2001) 4163–4166.
[4] S. Anna, N. Bontoux, H. Stone, Formation of dispersions using flow-focusing in microchannels, Appl. Phys. Lett. 82 (2003) 364.
[5] P. Garstecki, I. Gitlin, W. DiLuzio, G. Whitesides, E. Kumacheva, H. Stone, Formation of monodisperse bubbles in a microfluidic flow focusing device, Appl. Phys. Lett. 85 (2004) 2469.
[6] R. Dreyfus, P. Tabeling, H. Willaime, Ordered and disordered patterns in two-phase flows in microchannels, Phys. Rev. Lett. 90 (2003) 14.
[7] H. Song, J. Tice, R. Ismagilov, A microfluidic system for controlling reaction networks in time, Angew. Chem. 115 (2003) 792–796.
[8] S. Sugiura, M. Namajima, S. Iwamoto, M. Seki, Interfacial tension driven monodispersed droplet formation from microfabricated channel array, Langmuir 17 (2001) 5562–5566.
[9] Q. Xu, M. Nakajima, The generation of highly monodisperse droplets through the breakup of hydrodynamically focused microthread in a microfluidic device, Appl. Phys. Lett. 85 (2004) 3726–3728.
[10] P. Tabeling, A brief introduction to slippage, droplets and mixing in microfluidic systems, Lab Chip 9 (2009) 2428–2436.
[11] J. de Jong, M. Geerken, R. Lammertink, M. Wessling, Porous microfluidic devices-fabrication and applications, Chem. Eng. Technol. 30 (2007) 309–315.
[12] H. Fogler (Ed.), Elements of Chemical Reaction Engineering, 3rd edition, Prentice Hall and Englewood Cliffs, New Jersey, 1999.
[13] V. Hessel, H. Löwe, F. Schönfeld, Micromixers – A review on passive and active mixing principles, Chem. Eng. Sci. 60 (2005) 2479–2501.
[14] A. Gavriilidis, P. Angeli, E. Cao, K. Yeong, Y. Wan, Technology and applications of microengineered reactors, Chem. Eng. Res. Des. 80 (2002) 3–30.
[15] N. Nguyen, Z. Wu, Micromixers—a review, J. Micromech. Microeng. 15 (2005) R1–R16.
[16] A. Sudarshan, V. Ugaz, Fluid mixing in planar spiral microchannels, Lab Chip 6 (2006) 74–82.
[17] H. Winzeler, G. Belfort, Enhanced performance for pressure-driven membrane processes: the argument for fluid instabilities, J. Membr. Sci. 80 (1993) 35–47.
[18] H. Aref, S. Jones, S. Mofina, I. Zawadski, Vortices, kinematics and chaos, Physica D 37 (1989) 423–440.
[19] S. Jones, O. Thomas, H. Aref, Chaotic advection by laminar flow in a twisted pipe, J. Fluid Mech. 209 (1989) 335–357.
[20] P. Mishra, S. Gupta, Momentum transfer in curved pipes. 1. Newtonian fluids, Ind. Eng. Chem. Process Des. Dev. 18 (1979) 130–137.
[21] L. Austin, J. Seader, Fully developed viscous flow in coiled circular pipes, AIChE J. 19 (1973) 85–94.

[22] F. Jiang, K. Drese, S. Hardt, M. Küpper, F. Schönfeld, Helical flows and chaotic mixing in curved micro channels, AIChE J. 50 (2004) 2297–2305.
[23] S. Kim, S. Lee, Measurement of Dean flow in a curved micro-tube using micro digital holographic particle tracking velocimetry, Exp. Fluids 46 (2009) 255–264.
[24] A. Gigras, S. Pushpavanam, Early induction of secondary vortices for micromixing enhancement, Microfluid. Nanofluid. 5 (2008) 89–99.
[25] S. Schnabel, P. Moulin, Q. Nguyen, D. Roizard, P. Aptel, Removal of volatile organic components (VOCs) from water by pervaporation: separation improvement by Dean vortices, J. Membr. Sci. 142 (1998) 129–141.
[26] P. Moulin, J. Rouch, C. Serra, M. Clifton, P. Aptel, Mass transfer improvement by secondary flows: Dean vortices in coiled tubular membranes, J. Membr. Sci. 114 (1996) 235–244.
[27] R. Moll, D. Veyret, F. Charbit, P. Moulin, Dean vortices applied to membrane process – Part II: numerical approach, J. Membr. Sci. 288 (2007) 321–335.
[28] P. Moulin, D. Veyret, F. Charbit, Dean vortices: comparison of numerical simulation of shear stress and improvement of mass transfer in membrane processes at low permeation fluxes, J. Membr. Sci. 183 (2001) 149–162.
[29] J. Ghogomu, C. Guigui, J. Rouch, M. Clifton, P. Aptel, Hollow-fibre membrane module design: comparison of different curved geometries with Dean vortices, J. Membr. Sci. 181 (2001) 71–80.
[30] N. Scott Lynn, D. Dandy, Geometrical optimization of helical flow in grooved micromixers, Lab Chip 7 (2007) 580–587.
[31] C. Cortes-Quiroz, M. Zangeneh, A. Goto, On multiobjective optimization of geometry of staggered herringbone micromixer, Microfluid. Nanofluid. 7 (2009) 29–43.
[32] A. Mouza, C.-M. Patsa, F. Schönfeld, Mixing performance of a chaotic micromixer, Chem. Eng. Res. Des. 86 (2008) 1128–1134.
[33] A. Atkinson, A. Donev, R. Tobias (Eds.), Optimum Experimental Designs, Oxford University Press, New York, 2007, ISBN: 978-0-19-929659-0.